Original Article

G9a promotes inflammation in *Streptococcus pneumoniae* induced pneumonia mice by stimulating M1 macrophage polarization and H3K9me2 methylation in FOXP1 promoter region

Yi Li[1]^, Guanhua Li[1], Li Zhang[1], Yuechuan Li[1], Zhan Zhao[2]

[1]Department of Respiratory and Critical Care Medicine, Tianjin Chest Hospital, Tianjin, China; [2]Graduate School, Tianjin Medical University, Tianjin, China

Contributions: (I) Conception and design: Yi Li, G Li, Yuchuan Li; (II) Administrative support: None; (III) Provision of study materials or patients: Yi Li, Z Zhao; (IV) Collection and assembly of data: Yi Li, Z Zhao; (V) Data analysis and interpretation: Yi Li, L Zhang, Z Zhao; (VI) Manuscript writing: All authors; (VII) Final approval of manuscript: All authors.

Correspondence to: Yi Li. Department of Respiratory and Critical Care Medicine, Tianjin Chest Hospital, No. 261 Taierzhuang North Road, Jinnan District, Tianjin 300222, China. Email: lisalie5252@hotmail.com. Yuechuan Li. Department of Respiratory and Critical Care Medicine, Tianjin Chest Hospital, No. 261 Taierzhuang North Road, Jinnan District, Tianjin 300222, China. Email: liyuechuandoctor@126.com.

Background: *Streptococcus pneumoniae* has become a leading cause of pneumonia in recent years. Here, we investigated the mechanism of histone methylase G9a in *Streptococcus pneumoniae*-induced pneumonia (Spn).

Methods: G9a expression in Spn mouse tissue was measured. G9a lentivirus interference vector was injected into Spn mice to evaluate the wet and dry weight of the right upper lobe and the total lung water content (TLW) and wet/dry ratio (W/D). The number of neutrophils, macrophages, and lymphocytes in bronchoalveolar lavage fluid (BALF) was detected, and the levels of interleukin-1β (IL-1β), IL-6, tumor necrosis factor-α (TNF-α), and IL-10 in BALF were assessed. The expressions of M1 and M2 macrophage markers were also detected. The enrichment of histone 3 lysine 9 dimethylation (H3K9me2) in the Forkhead Box P1 (FOXP1) promoter was detected by chromatin immunoprecipitation (ChIP) assay, and the transcription level of FOXP1 was detected. Mouse macrophage RAW264.7 was induced by lipopolysaccharide (LPS) following G9a interference.

Results: G9a in the lung tissue of Spn mice was increased. After G9a knockdown, the mouse weight increased, the infiltration of inflammatory cells was decreased, levels of pro-inflammatory cytokines in BALF were decreased, CD86 and inducible nitric oxide synthase (iNOS) were decreased, and CD206 and arginase-1 (Arg-1) were elevated. In LPS-induced RAW264.7, G9a inhibited macrophage polarization to M1 and promoted macrophage polarization to M2. G9a promoted H3K9me2 methylation in the FOXP1 promoter region and inhibited its transcription, while FOXP1 downregulation reversed the inhibition of G9a knockdown on macrophage polarization to M1 and the inflammatory effect on Spn mice.

Conclusions: G9a promotes M1 polarization of macrophages by promoting H3K9me2 methylation in the FOXP1 promoter region, promoting an inflammatory response in Spn mice.

Keywords: *Streptococcus pneumoniae*; G9a; Forkhead Box P1 (FOXP1); histone 3 lysine 9 dimethylation (H3K9me2); macrophage polarization

Submitted Mar 16, 2022. Accepted for publication May 17, 2022.
doi: 10.21037/atm-22-1884
View this article at: https://dx.doi.org/10.21037/atm-22-1884

^ ORCID: 0000-0001-6988-4447.

Introduction

As a gram-positive bacterial pathogen, *Streptococcus pneumoniae* can cause invasive pneumonia, meningitis, otitis media, bacteremia (1), and acute respiratory distress requiring mechanical ventilation (2). *Streptococcus pneumoniae* is a leading cause of pneumonia, mostly in children less than five years and elderly people (3). Pneumonia is fatal in HIV-infected patients due to rampant and systemic inflammation and failure to control microbial infection (4), and community-acquired pneumonia is characterized as an acute inflammation of the lung associated with the activation of macrophages and neutrophils (5). The secretion of proinflammatory cytokines such as interleukin-8 (IL-8) and IL-6 by respiratory epithelial cells induced by the infection of respiratory bacteria, contributes to the onset of pneumonia (1). Macrophages are a class of leukocytes with antigen presentation ability which actively participate in tissue remodeling, phagocytosis, and clearance of foreign substances and cell debris (6). Macrophages are categorized into classically activated (M1) which is triggered by pathogen-associated molecular patterns (PAMPs) such as lipopolysaccharide (LPS), bacterial or viral DNA, and some cytokines, leading to high pro-inflammatory cytokine (7) and alternatively activated (M2) types which is elicited by cytokines IL-4, IL-13, and transforming growth factor-β (TGF-β) and leads to the resolution of inflammation, tissue reorganization, and regeneration. The balance between M1/M2 states is required for proper pathogen elimination and efficient structural and functional recovery (8). However, the mechanism of macrophage polarization in *Streptococcus pneumoniae*-induced pneumonia (Spn) is elusive.

As epigenetics can change gene expression and lung inflammation by changing the lung environment after exposure, it is an important field to evaluate the disease process (9). Epigenetics is a process of gene regulation mainly mediated via DNA methylation and histone modification, which affects the accessibility of potential DNA to transcription regulators and possibly influences serious diseases (10). DNA methylation and histone modifications are the two major manifestations of epigenetics in transcriptional regulation and require specific enzymes to catalyze (11). G9a is a histone methyl transferase which catalyzes the methylation of histone 3 lysine 9 (H3K9) and histone 3 lysine 27 (H3K27) (12). Its main function is to demethylate histone 3 lysine 9 dimethylation (H3K9me2), and G9a-dependent H3K9me2 is associated with gene silencing and works by recruiting H3K9me2 binding proteins that block transcriptional activation (13). G9a levels are elevated in many cancers, and its selective inhibition is known to reduce cell growth and induce autophagy, apoptosis, and senescence (14). G9a has been reported to play pivotal roles in lung cancer and fibrosis (15,16), and histone methyltransferases G9a can manage lipid-induced M1 macrophage polarization by negatively regulating CD36 (17). The recent study demonstrated that anisodamine enhances macrophage M2 polarization through suppressing G9a-mediated interferon regulatory factor-4 (IRF4) silencing to alleviate LPS-induced acute lung injury (ALI) (18). From the perspective of inflammation reduction, G9a may play an important role in ALI/acute respiratory distress syndrome (ARDS), and is regarded as a potential therapeutic target in pneumonia or ALI/ARDS. Furthermore, as its expression pattern in pneumonia and mechanism in Spn-induced macrophage polarization is largely unknown, molecular, histochemical, and physiological experiments were carried out to investigate the mechanism of macrophage polarization mediated by histone methylase G9a in Spn mice, which indicated the novelty of our study. We present the following article in accordance with the ARRIVE reporting checklist (available at https://atm.amegroups.com/article/view/10.21037/atm-22-1884/rc).

Methods

Establishment of Spn mouse model

The standard strain of *Streptococcus pneumoniae* ATCC49619 was purchased from the Guangdong microbial strain Preservation Center. After resuscitation, *Streptococcus pneumoniae* was cultured in blood agar medium (50 mL/L CO_2 at constant 37 ℃) for 18 h, then scraped off from the agar plate surface and suspended in sterile normal saline. The bacterial concentration was adjusted to 1.5×10^8 colony-forming unit (CFU) mL for standby. Clean grade healthy female BALB/c mice (N=140, 4 to 6 weeks old, 18±1 g) were purchased from Hunan SJA Laboratory Animal Co., Ltd. (Changsha, Hunan, China). Housing and breeding of animals were performed humanely for 2 weeks with regard for the alleviation of suffering following the Chinese national guidelines for the care and use of animals. Animal experiments were approved by the Animal Ethics Committee of Tianjin Chest Hospital (No. TJCH-2021-010). A protocol was prepared before the study without registration.

A control group of 20 mice was selected (WT group), and other mice were used to establish the Spn model.

Twenty mice with successful modeling (Spn group) were selected for model identification, and the remaining 100 with successful modeling were arbitrarily assigned into five groups, with 20 mice in each group. A mock group (without any treatment after modeling), sh-NC group (injected with negative control of G9a lentiviral interference vector after modeling), sh-G9a group (injected with G9a lentiviral interference vector after modeling), sh-G9a group + sh-NC group (injected with negative controls of G9a lentivirus interference vector and FOXP1 lentivirus interference vector after modeling), and sh-G9a + sh-FOXP1 group (injected with G9a lentivirus interference vector and FOXP1 lentivirus interference vector after modeling) were established. The lentiviral vector was provided by the Shanghai Gemma Pharmaceutical Technology Co., Ltd, the viral titer was 1.0×10^9 TU/mL, and the injection volume was 3 μL (19).

All model mice were anesthetized by intraperitoneal injection of 3% pentobarbital sodium, and after the nasal mucosa was punctured with a sterile needle, 50 μL prepared bacterial solution was slowly dripped from the nasal cavity, and automatically inhaled. In the control group, 50 μL normal saline was dripped into the nasal cavity after the nasal mucosa was punctured. The weight of the 20 mice in each group was measured after infection. After the mice were sacrificed by intraperitoneal injection of pentobarbital sodium (100 mg/kg), the wet/dry weight ratio (W/D) and total lung water content (TLW) of the lung tissues of five mice were measured, and the lung tissues of six were selected for embedding and hematoxylin and eosin (HE) staining. The bronchoalveolar lavage fluid (BALF) of four mice was also selected, and the lung tissues of the remaining five were collected to prepare homogenate for reverse transcription quantitative polymerase chain reaction (RT-qPCR) and Western blot (WB) experiments (20).

HE staining

The lung tissue samples were washed with normal saline, fixed in 4% paraformaldehyde for 30–50 min, washed, dehydrated, cleared, immersed in wax, embedded, and sliced. After flattening, the tissue slices were pasted on glass slides, dried in a 45 ℃ incubator, dewaxed, dehydrated with high to low concentration alcohol, and washed with distilled water for 5 min. Samples were then stained with hematoxylin (517-28-2, Solarbio, Beijing, China) for 5 min, rinsed with running water for 3 s, differentiated using 1% hydrochloric acid ethanol for 3 s, stained with 5% eosin solution (17372-87-1, Solarbio) for 3 min, then dehydrated, cleared and sealed. Tissue sections were observed under a microscope.

BALF extraction

After the chest was dissected, the lung tissue was exposed and the trachea was cut, with the scalp needle used for tracheal intubation. After fixation with $0^{\#}$ silk thread, the lung tissue was quickly separated, the left main bronchus was ligated, and the right lung was subjected to lavage through the air tube. The right lung was then slowly washed with 1 mL normal saline via the tracheal intubation three times, and the lung tissue was gently massaged with fingers. After about 30 seconds, the BALF was selected and the recovery rate was over 80%. The recovered liquid was centrifuged at 2,000 rpm for 15 min, then the supernatant was separately packed in a cryopreservation tube and stored at -80 ℃. The number of neutrophils, macrophages, and lymphocytes in the BALF was counted.

Enzyme-linked immunosorbent assay (ELISA)

BALF was collected, and the expression of inflammatory factors was detected according to the instructions of IL-1β (MLB00C), tumor necrosis factor-α (TNF-α) (MTA00B), IL-6 (D6050), and IL-10 (DY417-05) ELISA kits (R&D systems, Minneapolis, MN, USA).

Cell culture and transfection

Mouse macrophage RAW264.7 was purchased from ATCC, thawed in 37 ℃ water bath heat, transferred to a 15 mL centrifuge tube, and centrifuged at 1,000 rpm for 5 min. The supernatant was discarded, and cells were resuspended. The cell suspension was dispersed to the culture flask and vibrated gently for a few times to let the cells evenly spread in the 25 cm^2 cell flask. Cells were then cultured at 37 ℃ in a 5% CO_2 incubator, and the medium was refreshed every 2 days. When cells reached 80–90% confluence (about 1×10^7), macrophages were treated with LPS (strain O55: B5, Sigma-Aldrich, St. Louis, MO, USA) and RAW264.7 cells were treated with 500 ng/mL LPS for 24 h.

RAW264.7 cells induced by LPS were infected with corresponding lentivirus (sh-G9a, sh-NC, sh-FOXP1) (Genechem, Shanghai, China), and the multiplicity of infection was 20 (21). After 48 h of infection, the following experiment was then carried out.

Table 1 Primer sequences of RT-qPCR

Primer	Sequence
G9a	F: 5'-TTCAGTCTCTACTATGATTTT-3'
	R: 5'-ATCATAGTAGAGACTGAATT-3'
iNOS	F; 5'-GCAAGCCCTCACCTACTTCC-3'
	R: 5'-AACCTC TGCCTGTGCGTCT-3'
Arg-1	F: 5'-AGACAGCAGAGGAGGTGAAGAGTAC-3'
	R: 5'-GGTAGTCAGTCCCTGGCTTATGGT-3'
FOXP1	F: 5'-TCCAGAAAAGCAGCTAACACTA-3'
	R: 5'-TTCTACTCGCACAAAACACTTG-3'
FOXP1 promoter	F: 5'-GGGGGATTAGCTGCTCAATACC-3'
	R: 5'-GTCATGGTGCATGTATGGAGG-3'
GAPDH	F: 5'-ATCCACGGGAGAGCGACAT-3'
	R: 5'-CAGCTGCTTGTAAAGTGGAC-3'

RT-qPCR, reverse transcription quantitative polymerase chain reaction.

RT-qPCR

Total RNA in rat myocardial tissue was extracted following the instructions of TRIzol reagent (15596026, Invitrogen). The concentration of total RNA was then quantified. Total RNA was reversely transcribed into cDNA using a PrimeScript RT reagent kit (RR047A, Takara, Dalian, China), and PCR was performed according to the instructions of a Fast SYBR Green PCR kit (Applied Biosystems) on an ABI PRISM 7300 qRT-PCR system (Applied biosystems). Three replicates were set for each well. GAPDH served as the internal reference, and the mRNA expression of each sample was calculated using $2^{-\Delta\Delta Ct}$ method. The primer sequences are shown in *Table 1* (22,23).

WB analysis

The total protein in tissues or cells was extracted by RIPA lysis (C0481, Sigma Aldrich, USA), lysed at 4 ℃ for 15 min, and centrifuged at 15,000 rpm for 15 min. The concentration was determined by bicinchoninic acid method (23227, Thermo, USA). The samples were subjected to gel electrophoresis, then moved into polyvinylidene fluoride membranes, which were blocked with 5% skim milk for 1 h, and incubated overnight with the primary antibodies (all from Abcam) against G9a (1:500, ab183889), FOXP1 (1:1,000, ab134055), GAPDH (1:5,000, ab8245). The next day, the membranes were rinsed with tris-buffered saline-tween containing 0.1% tween 20 and probed with secondary antibody IgG H&L-conjugated horseradish peroxidase (1:20,000, ab205718) for 1.5 h. The protein was developed by adding developer (NCI4106, pierce, Rockford, IL, USA). ImageJ 1.48u software (Bio-Rad, Hercules, CA, USA) was used for protein quantitative analysis, and the ratio of gray value of each protein to gray value of GAPDH was used for protein quantitative analysis. Each experiment was repeated three times.

Flow cytometry

The tissue was cut into 1 mm^3 pieces, washed repeatedly with PBS, then detached with 1.5 mL 0.25% dispersase, 0.5 mL 0.4% collagenase, and 50 μL fetal bovine serum at 4 ℃ overnight for 12–16 h. The tissue was then detached in a 37 ℃ incubator for 30 min, the cell suspension was collected and filtered with 300-mesh nylon mesh to remove the cell mass, and the cell debris removed by centrifugation. The cells were made into single cell suspension and resuspended in staining buffer (BD Biosciences). FSC and SSC were used as coordinates to remove cell debris and doublets, then PI was used to stain the cells, and PI and FSC were used to set a gate to label living cells The cells were stained with F4/80 (17-4801-82, 1:50, eBioscience, San Diego, CA, USA), CD86 (25-0862-82, 1:400, eBioscience), and CD206 (12-2061-82, 1:800, eBioscience), then detected by flow cytometry BD FACS canto II (BD immunocytometry systems), and analyzed by Flow Jo software 7.6.

Chromatin immunoprecipitation (ChIP)

Upon 70–80% confluence, the cells were fixed with 1% formaldehyde for 10 min to make the DNA and protein in the cell cross-linked. After crosslinking, the cells were randomly broken by ultrasonic treatment, 10 s each time with an interval of 10 s and 15 cycles, to break them into 200 bp fragments. Cells were then centrifuged at 4 ℃ for 10,000 ×g, and the supernatant was collected and divided into two tubes, which were respectively added with the negative control antibody rabbit anti-IgG (ab109489, 1:100, Abcam) and the target protein specific antibody rabbit anti-H3K9 (1:100, ab1220, Abcam) overnight at 4 ℃. The endogenous DNA-protein complex was precipitated by Protein Agarose/Sepharose, and the supernatant was discarded after a short centrifugation. The nonspecific complex was washed and decross-linked overnight at 65 ℃,

and the DNA fragment was extracted and purified by phenol/chloroform overnight. The enrichment of H3K9 in the FOXP1 promoter fragment was detected by RT-qPCR with FOXP1 promoter fragment specific primers.

Statistical analysis

SPSS 21.0 (IBM Corp. Armonk, NY, USA) was employed for data analysis, and data are shown in mean ± standard deviation (SD). The *t* test was used for analyzing comparisons between two groups, one-way analysis of variance (ANOVA) for comparing different groups, and Tukey's multiple comparison test was used for pairwise comparisons after ANOVA. The data of each group at different time points were compared by repeated measurement ANOVA, and $P<0.05$ indicated a statistically significant difference.

Results

G9a is upregulated in Spn mice

Previous study has shown that overexpression of G9a significantly promotes the proliferation and invasion of NSCLC cells, and while knockout of G9a inhibited the growth and metastasis of NSCLC cells *in vivo* (24), its role in Spn has not been reported. Compared with wild-type mice, the weight of Spn mice was significantly reduced (*Figure 1A*). The wet weight (W) and dry weight (D) of the right upper lobe were measured and TLW and W/D were calculated, and compared with the WT group, W/D and TLW (*Figure 1B*) in the Spn group were enhanced significantly. HE staining was used to observe the pathological changes of lung tissue after *Streptococcus pneumoniae* infection. In the WT group, the pathological condition of lung tissue and alveolar septum were normal, while in the Spn group, the alveolar structure was seriously damaged, the alveolar septum was significantly widened, the tracheal epithelium was exfoliated, and many inflammatory cells were exuded (*Figure 1C*). The number of neutrophils, macrophages, and lymphocytes in the BALF after *Streptococcus pneumoniae* infection was higher in the Spn group than in the WT group (*Figure 1D*). ELISA results elicited that the levels of IL-1β, IL-6, and TNF-α in the BALF of Spn mice were increased, while IL-10 was decreased (*Figure 1E*). The expression of *G9a* in the lung tissue of Spn mice was then detected, and compared with WT mice, was clearly increased ($P<0.05$) (*Figure 1F*). These results indicate G9a is related to Spn.

G9a knockdown has a protective effect on Spn mice

To explore whether G9a is involved in the disease progression of Spn in mice, we used sh-G9a lentiviral vector to interfere with G9a in mice and used RT-qPCR and WB experiment to detect its interference efficiency (*Figure 2A*). After *G9a* knockdown, the weight of mice was increased significantly (*Figure 2B*), and W/D and TLW were evidently reduced (*Figure 2C*). HE staining showed that after *G9a* knockdown, the pathological changes of lung tissue were qualitatively different, the infiltration of inflammatory cells was reduced, and the alveolar septum was basically restored to normal (*Figure 2D*). The number of neutrophils, macrophages, and lymphocytes were clearly lowered after *G9a* knockdown (*Figure 2E*), and ELISA results demonstrated that compared with the sh-NC group, levels of IL-1β, IL-6, and TNF-α in the BALF of the sh-G9a group were decreased, while IL-10 was elevated (*Figure 2F*). These results suggest *G9a* knockdown promotes the anti-inflammatory effect of Spn in mice.

G9a knockdown promotes the polarization of pulmonary macrophages from M1 pro-inflammatory phenotype to M2 anti-inflammatory phenotype

Macrophages are the first line of defense against pathogens. When they encounter invading pathogens, they will carry out phagocytosis, transfer excessive pro-inflammatory and anti-inflammatory cytokines, and shape the tissue microenvironment. During the whole process of pneumonia, alveolar macrophages and infiltrating monocytes produce increasing numbers of cytokines which activate antiviral/antibacterial immunity but may also trigger a so-called cytokine "storm" and the risk of normal tissue damage (25). Macrophages can generally differentiate into M1 and M2 phenotype (26), and to further explore whether *G9a* could affect the polarization of pulmonary macrophages *in vivo*, we detected the expression of CD86 on M1 macrophages and CD206 on M2 macrophages in lung tissue by flow cytometry. Compared with the sh-NC group, CD86 in the sh-G9a group was notably decreased and CD206 was increased (*Figure 3A*). RT-qPCR was used to detect the expression of M1 macrophage marker inducible nitric oxide synthase (*iNOS*) and M2 macrophage marker *Arg-1*, and it was found that *iNOS* was lowered and *Arg-1* was elevated after *G9a* knockdown (*Figure 3B*). Briefly, *G9a* knockdown

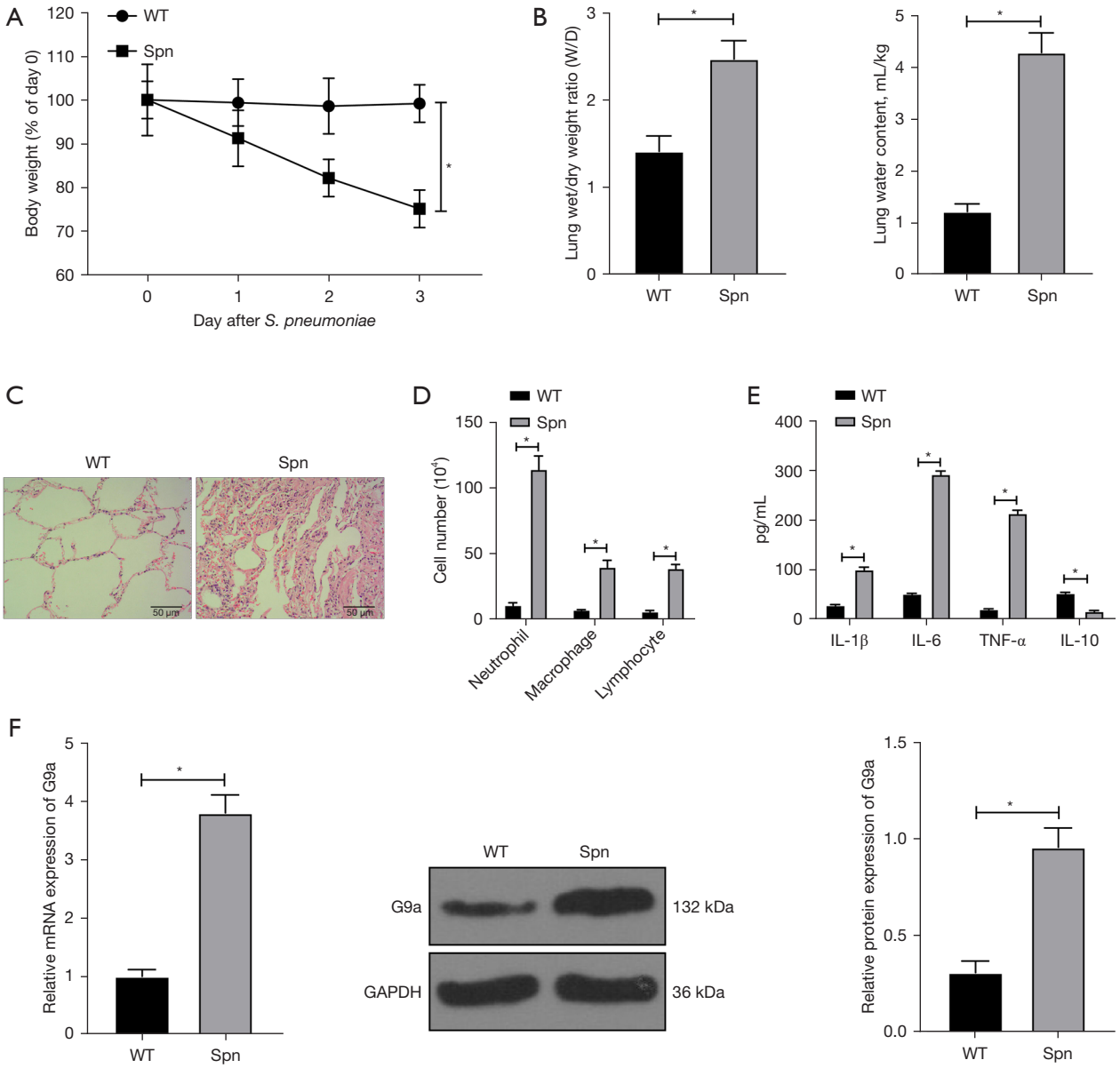

Figure 1 G9a is highly expressed in the mouse model of *Streptococcus pneumoniae* induced pneumonia induced by *Streptococcus pneumoniae* infection. (A) Weight change of mice (N=20 in each group); (B) W/D of right upper lobe tissue were measured, TLW and W/D were calculated (N=5 in each group); (C) HE staining was used to observe the pathological changes of lung tissue after *Streptococcus pneumoniae* infection (N=6 in each group); (D) the number of neutrophils, macrophages, and lymphocytes in BALF (N=4 in each group); (E) ELISA measured levels of IL-1β, IL-6, TNF-α, and IL-10 in BALF after *Streptococcus pneumoniae* infection (N=4 in each group); (F) RT-qPCR and WB were used to detect the expression of G9a in lung tissue of mice infected with *Streptococcus pneumoniae* (N=5 in each group). The data are expressed as mean ± SD; independent sample *t* test was used for comparison between two groups; and repeated measurement analysis of variance was used for data comparison between two groups at different time points; *, P<0.05. TLW, total lung water content; W/D, wet/dry weight ratio; WT, wild type; Spn, *Streptococcus pneumoniae*-induced pneumonia; HE staining, hematoxylin-eosin staining; ELISA, enzyme-linked immunosorbent assay; IL-1β, interleukin-1β; IL-6, interleukin-6; TNF-α, tumor necrosis factor-α; IL-10, interleukin-10; BALF, bronchoalveolar lavage fluid; RT-qPCR, reverse transcription quantitative polymerase chain reaction; WB, Western blot; SD, standard deviation.

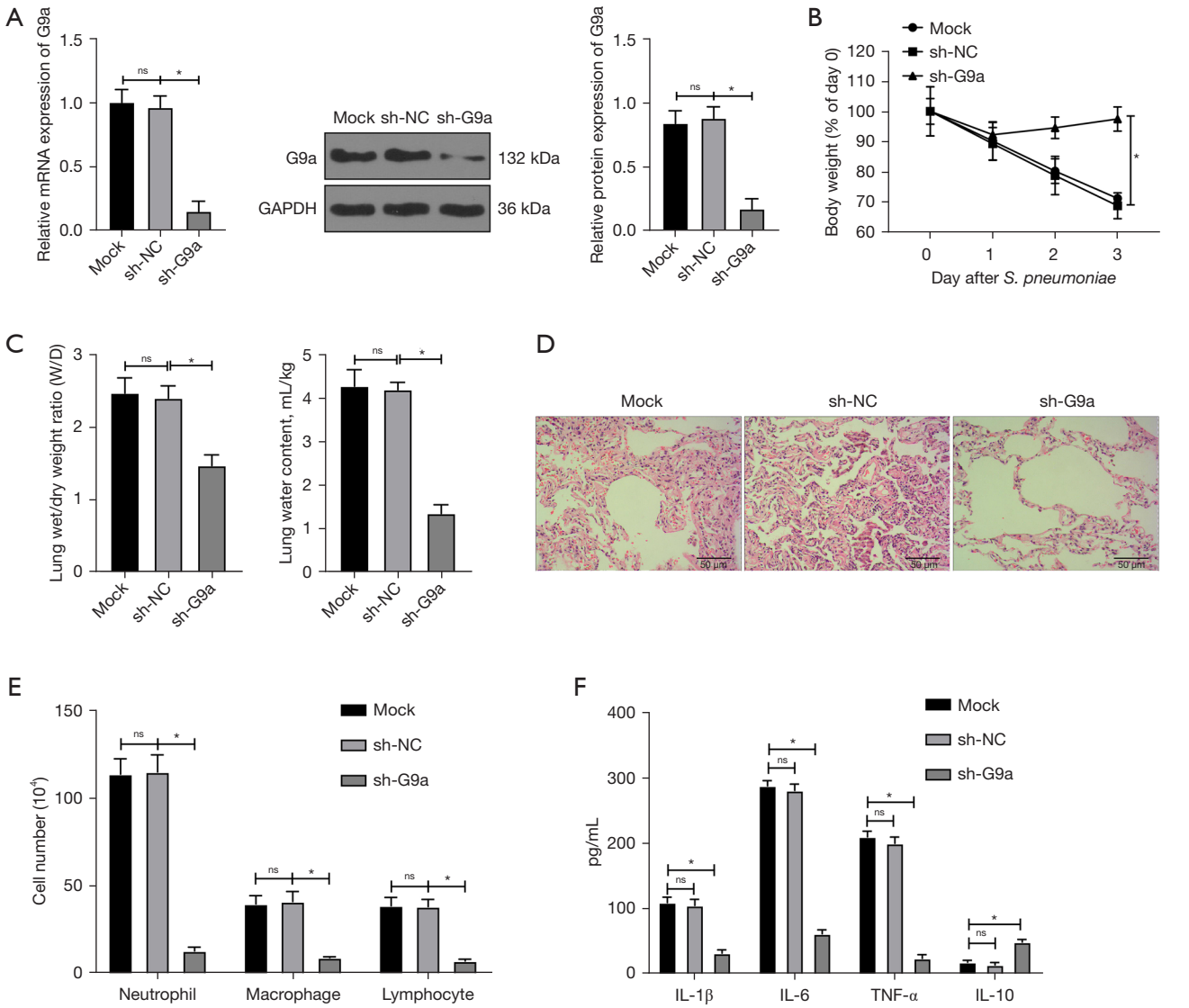

Figure 2 G9a knockdown affects the inflammatory response induced by *Streptococcus pneumoniae* in mice. Lentiviral vector interfering with G9a was injected into a *Streptococcus pneumoniae* induced pneumonia mouse model. (A) RT-qPCR and WB test were used to detect the interference efficiency of G9a (N=5 in each group); (B) weight change of mice (N=20 in each group); (C) wet weight and dry weight of right upper lobe tissue were measured and TLW and W/D were calculated (N=5 in each group); (D) HE staining was used to observe the pathological changes of lung tissue after *Streptococcus pneumoniae* infection (N=6 in each group); (E) the number of neutrophils, macrophages, and lymphocytes in BALF (N=4 in each group); (F) ELISA measured levels of IL-1β, IL-6, TNF-α, and IL-10 in BALF after *Streptococcus pneumoniae* infection (N=4 in each group). The data are expressed as mean ± SD; one-way ANOVA and Tukey's post hoc test were used for comparison among multiple groups; and repeated measurement analysis of variance was used for data comparison between two groups at different time points; *, P<0.05. TLW, total lung water content; W/D, wet/dry weight ratio; HE staining, hematoxylin-eosin staining; RT-qPCR, reverse transcription quantitative polymerase chain reaction; WB, Western blot; ELISA, enzyme-linked immunosorbent assay; IL-1β, interleukin-1β; IL-6, interleukin-6; TNF-α, tumor necrosis factor-α; IL-10, interleukin-10; BALF, bronchoalveolar lavage fluid; SD, standard deviation; ANOVA, analysis of variance; ns, no significance.

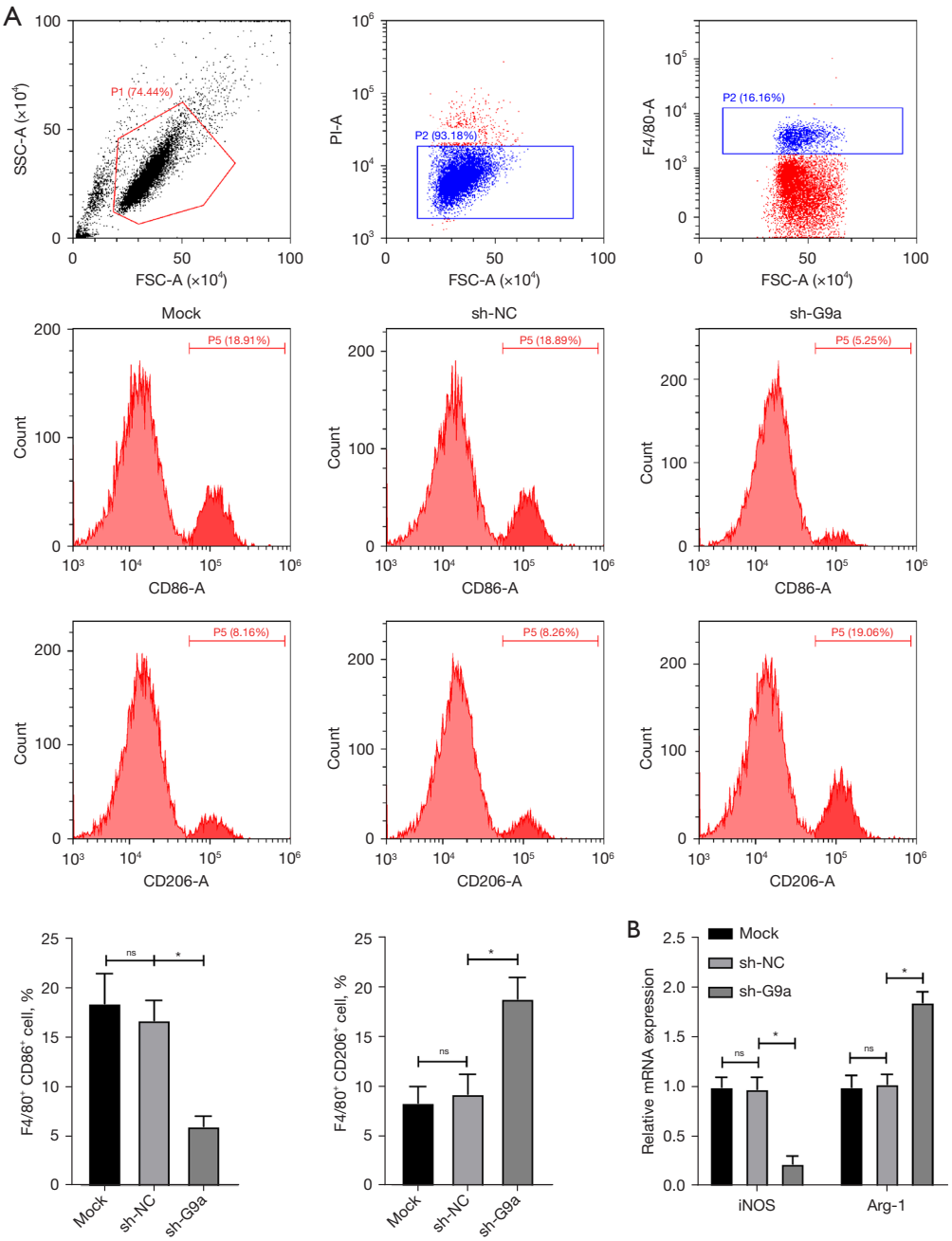

Figure 3 G9a knockdown can promote the polarization of pulmonary macrophages from M1 pro-inflammatory phenotype to M2 anti-inflammatory phenotype. G9a lentivirus interference vector was injected into a *Streptococcus pneumonia*-induced pneumonia mouse model. (A) Surface markers of M1 macrophages CD86 and M2 macrophages CD206 were detected by flow cytometry. Firstly, cell debris (black dots out of frame) were removed by FSC and SSC, then living (blue dots) and dead (red dots) cells were distinguished by PI labeling. Finally, M1 and M2 macrophages were sorted out by F4/80 (blue dots), CD86, and CD206. The percentage of all cells refers to the percentage of living cells; (B) the expression of M1 macrophage markers iNOS and M2 macrophage markers Arg-1 were detected by RT-qPCR (N=5 in each group). The data are expressed as mean ± SD; and one-way ANOVA and Tukey's post hoc test was used for comparison among multiple groups. *, P<0.05. RT-qPCR, reverse transcription quantitative polymerase chain reaction. FSC, forward scatter; SSC, side scatter; PI, propidium iodide; iNOS, inducible nitric oxide synthase; Arg-1, Arginase-1; RT-qPCR, reverse transcription quantitative polymerase chain reaction; SD, standard deviation; ANOVA, analysis of variance; ns, no significance.

inhibits the polarization of M1 macrophages and promotes the polarization of M2 macrophages *in vivo*.

G9a knockdown promotes the LPS-induced mouse macrophage line RAW264.7 to polarize from M1 pro-inflammatory phenotype to M2 anti-inflammatory phenotype

To further verify the regulatory effect of *G9a* on macrophages *in vitro*, RAW264.7 macrophages were allocated into the control group, LPS + Mock group, LPS + sh-NC group, and LPS + sh-G9a group, and RT-qPCR and WB showed that *G9a* interference was successful (*Figure 4A*). Flow cytometry showed CD86 was decreased and CD206 was increased significantly after *G9a* knockdown (*Figure 4B*), while RT-PCR noted *iNOS* was decreased and *Arg-1* was increased significantly (*Figure 4C*). These results suggest *G9a* knockdown *in vitro* can significantly promote the polarization of the LPS-induced RAW264.7 macrophage line from M1 pro-inflammatory phenotype to M2 anti-inflammatory phenotype.

G9a promotes the methylation of H3K9me2 in FOXP1 promoter and inhibits its transcription

The above results indicate *G9a* can affect the inflammatory response *in vivo* and *in vitro* by regulating macrophage polarization. To further explore the downstream mechanism of *G9a*, we looked for references and found that G9a inhibits FOXP1 by promoting H3K9me2 methylation in non-small cell lung cancer (15). As FOXP1 is related to pathogen induction, neutrophil and macrophage recruitment, and the inflammatory process (27), we speculated G9a might affect pneumonia through epigenetic regulation of FOXP1 transcription in Spn mice. To validate the above conjecture, we first detected the enrichment of H3K9me2 in the FOXP1 promoter region in RAW264.7 macrophages after *G9a* overexpression and depletion by ChIP experiment, and the results showed this was increased significantly after *G9a* overexpression and decreased after *G9a* depletion (*Figure 5A*). In addition, when Bix01294 [specifically inhibiting G9a (H3K9me2)] was added to cells, the ChIP experiment showed enrichment of H3K9me2 in the FOXP1 promoter region was evidently inhibited (*Figure 5B*). RT-qPCR showed FOXP1 was decreased after *G9a* overexpression, and FOXP1 transcription was increased significantly after *G9a* depletion (*Figure 5C*). FOXP1 expression in lung tissue after *Streptococcus pneumoniae* infection was then examined by RT-qPCR, and compared with the WT group, FOXP1 was decreased in the Spn group, while clearly increased after *G9a* depletion (*Figure 5D*). RT-qPCR showed FOXP1 was increased in cells after *G9a* depletion (*Figure 5E*). Overall, G9a inhibits FOXP1 transcription by promoting H3K9me2 methylation in the FOXP1 promoter.

Silencing FOXP1 reverses the inhibitory effect of G9a knockdown on M1 macrophages

To further study whether *G9a* affected macrophage polarization by inhibiting FOXP1 transcription, we set the following groups for macrophage RAW264.7: sh-G9a group, sh-G9a + sh-NC group, and sh-G9a + sh-FOXP1 group. First, the efficiency of intracellular FOXP1 interference was verified by RT-qPCR (*Figure 6A*). Flow cytometry revealed that compared with the sh-G9a + sh-NC group, CD86 on the surface of M1 macrophages was increased and CD206 on the surface of M2 macrophages was significantly decreased in the sh-G9a + sh-FOXP1 group (*Figure 6B*). RT-qPCR elicited *iNOS* was increased and *Arg-1* was significantly decreased after simultaneously interfering with *G9a* and FOXP1 (*Figure 6C*). Taken together, FOXP1 silencing *in vitro* can avert the inhibitory effect of *G9a* knockdown on M1 macrophages.

Silencing FOXP1 reverses the protective effect of G9a knockdown on Spn mice

We further verified that *G9a* is involved in the disease progression of Spn in mice by regulating FOXP1. We divided mice into a sh-G9a group, sh-G9a + sh-NC group, and sh-G9a + sh-FOXP1 group, and used RT-PCR to verify the interference efficiency of sh-FOXP1 (*Figure 7A*). Compared with the sh-G9a + sh-FOXP1 group, the weight of mice in the sh-G9a + sh-NC group was significantly reduced (*Figure 7B*), pathological injury of lung tissue was aggravated, inflammatory cell infiltration was increased (*Figure 7C*), levels of IL-1β, IL-6, and TNF-α in the BALF were increased, levels of IL-10 were decreased (*Figure 7D*), CD86 was increased, CD206 was decreased (*Figure 7E*), *iNOS* was increased, and *Arg-1* was decreased (*Figure 7F*). Collectively, FOXP1 silencing *in vivo* can avert the protective effect of *G9a* depletion on Spn mice.

Discussion

Epigenetic changes such as DNA methylation and

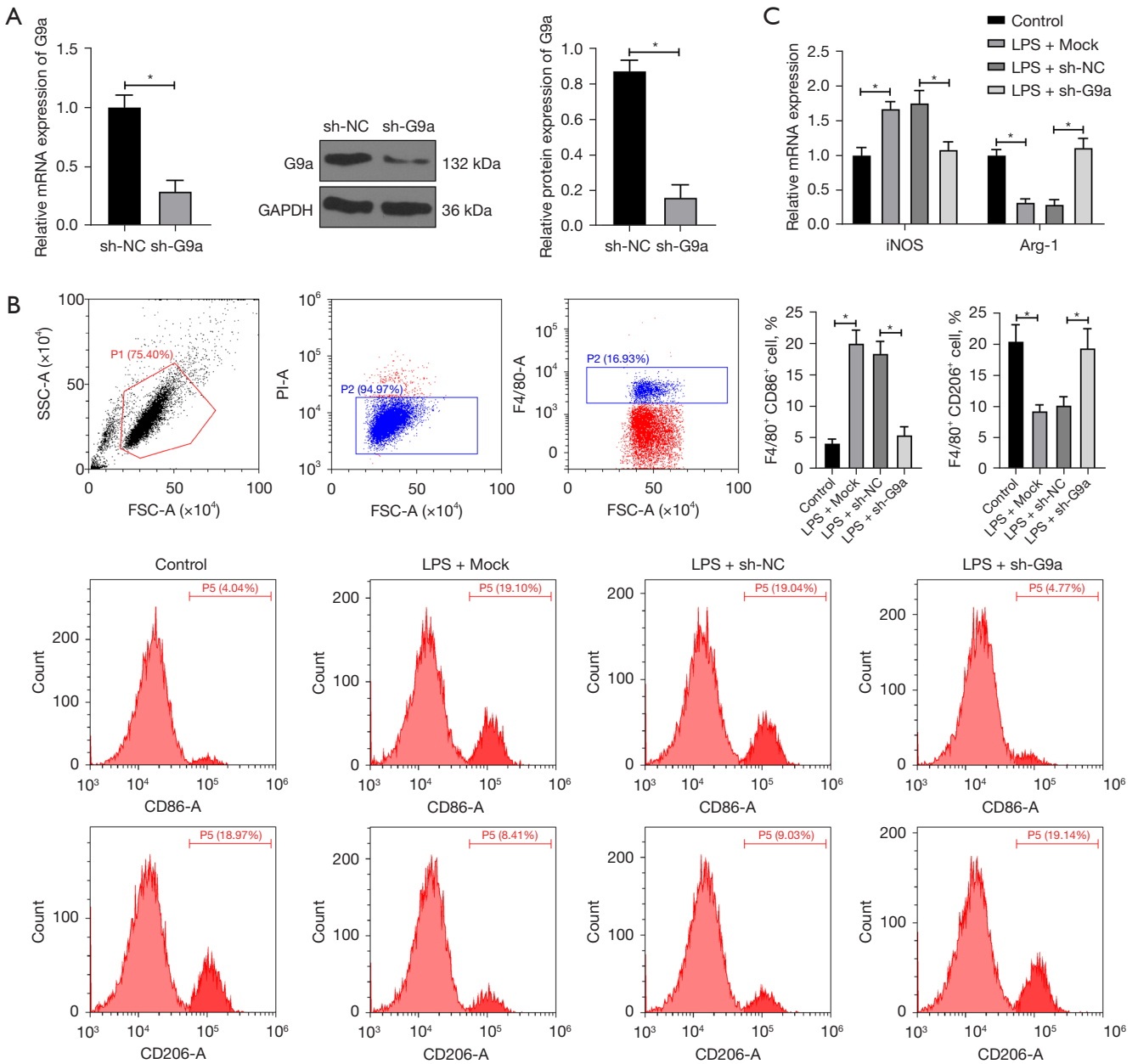

Figure 4 G9a knockdown can promote the polarization of LPS-induced RAW264.7 macrophage line from M1 pro-inflammatory phenotype to M2 anti-inflammatory phenotype. G9a lentivirus interference vector was infected into LPS-induced RAW264.7 macrophage line. (A) RT-qPCR and WB test were used to detect G9a expression in cells; (B) the surface markers of M1 macrophages CD86 and M2 macrophages CD206 were detected by flow cytometry. Firstly, cell debris (black dots out of frame) were removed by FSC and SSC, then living (blue dots) and dead (red dots) cells were distinguished by PI labeling. Finally, M1 and M2 macrophages were sorted out by F4/80 (blue dots), CD86, and CD206. The percentage of all cells refers to the percentage of living cells; (C) the expression of M1 macrophage markers iNOS and M2 macrophage markers Arg-1 were detected by RT-qPCR. The experiment was repeated three times. The data are expressed as mean ± SD; and one-way ANOVA and Tukey's post hoc test was used for comparison among multiple groups; *, P<0.05. LPS, lipopolysaccharide; RT-qPCR, reverse transcription quantitative polymerase chain reaction; WB, Western blot; FSC, forward scatter; SSC, side scatter; PI, propidium iodide; iNOS, inducible nitric oxide synthase; Arg-1, Arginase-1; SD, standard deviation; ANOVA, analysis of variance.

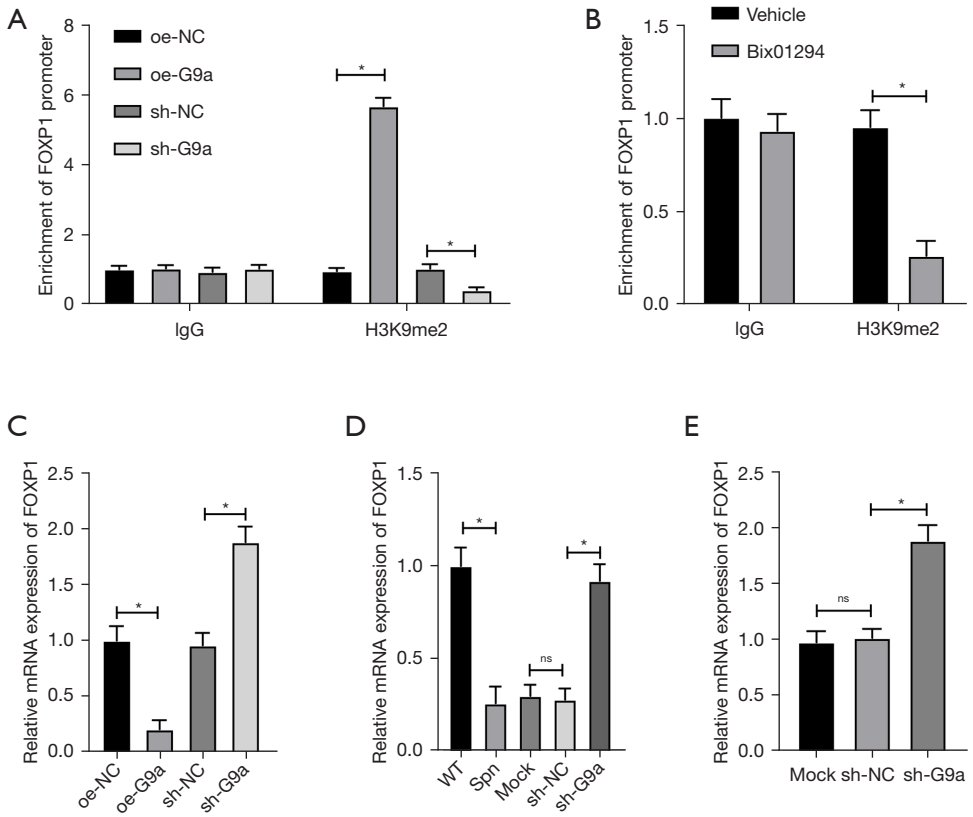

Figure 5 G9a affects FOXP1 transcription through epigenetic effects. (A) The enrichment of H3K9me2 in FOXP1 promoter region was detected by ChIP assay after G9a overexpression and interference; (B) the enrichment of H3K9me2 in the FOXP1 promoter region was detected by ChIP assay after Bix01294 was added into cells; (C) FOXP1 expression was detected by RT-qPCR after G9a interference and G9a overexpression; (D,E) RT-qPCR was used to detect FOXP1 expression after G9a interference *in vivo* and *in vitro* (N=5 in each group). The experiment was repeated three times. The data are expressed as mean ± SD; independent sample *t* test was used for comparison between two groups; and one-way ANOVA and Tukey's post hoc test was used for comparison among multiple groups; *, P<0.05. H3K9me2, histone 3 lysine 9 dimethylation; FOXP1, Forkhead Box P1; ChIP, chromatin immunoprecipitation; RT-qPCR, reverse transcription quantitative polymerase chain reaction; WT, wild type; Spn, *Streptococcus pneumoniae*-induced pneumonia; SD, standard deviation; ANOVA, analysis of variance; ns, no significance.

histone modification are known to modulate gene expression changes and impact cellular function (28,29). As an epigenetic modifier, G9a has been documented to participate in many diseases (30,31) but its expression pattern and mechanism in Spn is largely unknown. This study investigated the mechanism of macrophage polarization mediated by histone methylase G9a in Spn mice, and eventually supported that G9a promoted M1 macrophage polarization by promoting H3K9me2 methylation in the FOXP1 promoter region, stimulating inflammation in Spn mice (*Figure 8*).

While G9a is implicated in lung cancer stemness through epigenetic modification of DNA methylation maintenance of several cancer stem cell genes (15), its role in Spn has not been documented. In this study, a mouse model of pneumonia was induced by *Streptococcus pneumoniae* infection, and compared with wild-type mice, G9a in the lung tissue of Spn mice was clearly increased. To explore G9a action in Spn progression, we used sh-G9a lentiviral vector to silence *G9a* in mice, and found after its knockdown, the weight of Spn mice was increased, W/D and TLW were evidently reduced, the pathological changes of lung tissue were qualitatively different, the infiltration of inflammatory cells was reduced, and the alveolar septum was restored to normal. The number of neutrophils, macrophages, and lymphocytes were lowered clearly, and the levels of IL-1β, IL-6, and TNF-α

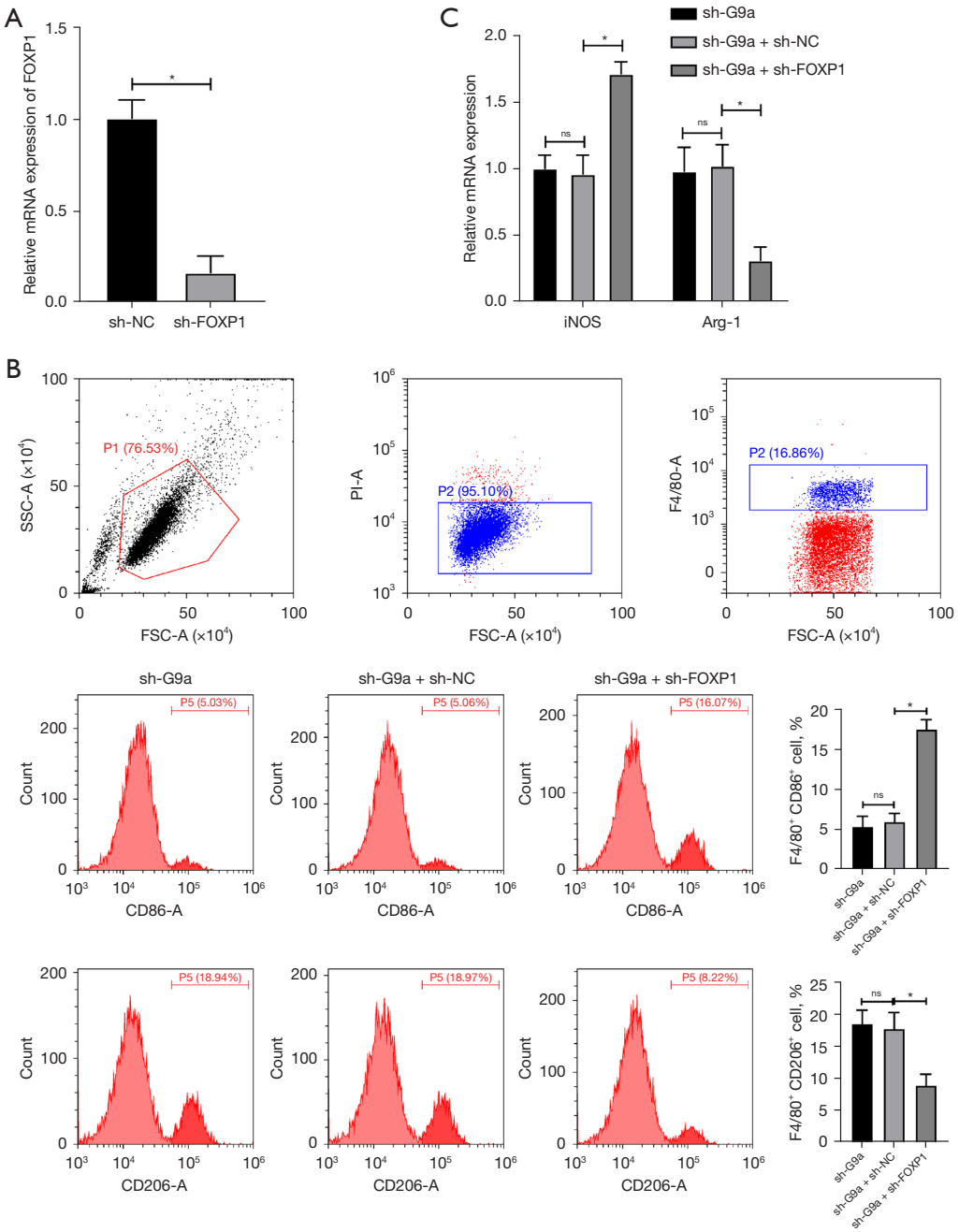

Figure 6 G9a affects RAW264.7 polarization of macrophages by regulating FOXP1 expression *in vitro*. Macrophage RAW264.7 was transfected with G9a and FOXP1 lentiviral interference vectors at the same time. (A) The interference efficiency of FOXP1 was detected by RT-qPCR; (B) the surface markers of M1 macrophages CD86 and M2 macrophages CD206 were detected by flow cytometry. Firstly, cell debris (black dots out of frame) were removed by FSC and SSC, and then living (blue dots) and dead (red dots) cells were distinguished by PI labeling. Finally, M1 and M2 macrophages were sorted out by F4/80 (blue dots), CD86 and CD206. The percentage of all cells refers to the percentage of living cells; (C) the expression of M1 macrophage markers iNOS and M2 macrophage markers Arg-1 were detected by RT-qPCR. The experiment was repeated three times. The data are expressed as mean ± SD; and one-way ANOVA and Tukey's post hoc test was used for comparison among multiple groups; *, P<0.05. FOXP1, Forkhead Box P1; RT-qPCR, reverse transcription quantitative polymerase chain reaction; FSC, forward scatter; SSC, side scatter; PI, propidium iodide; iNOS, inducible nitric oxide synthase; Arg-1, Arginase-1; SD, standard deviation; ANOVA, analysis of variance; ns, no significance.

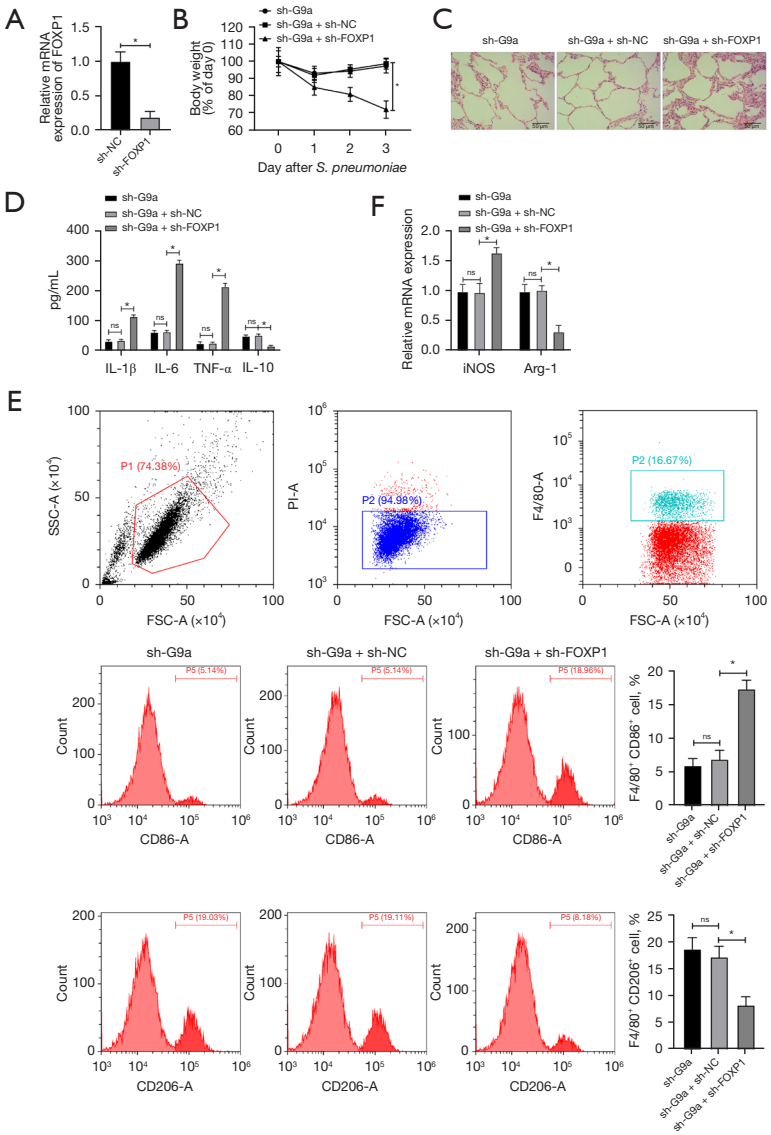

Figure 7 G9a affects macrophage polarization and inflammatory response by regulating FOXP1 expression *in vivo*. G9a and FOXP1 lentiviral interference vectors were simultaneously transfected into *Streptococcus pneumoniae* induced pneumonia mice; (A) RT-qPCR was used to detect FOXP1 interference efficiency *in vivo* (N=5 in each group); (B) weight change of mice (N=20 in each group); (C) HE staining was used to observe the pathological changes of lung tissue after *Streptococcus pneumoniae* infection (N=6 in each group); (D) ELISA measured levels of IL-1β, IL-6, TNF-α and IL-10 in BALF (N=4 in each group); (E) the surface markers of M1 macrophages CD86 and M2 macrophages CD206 were detected by flow cytometry (N=5 in each group). Firstly, cell debris (black dots out of frame) were removed by FSC and SSC, then living (blue dots) and dead(red dots) cells were distinguished by PI labeling. Finally, M1 and M2 macrophages were sorted out by F4/80 (green dots), CD86 and CD206. The percentage of all cells refers to the percentage of living cells; (F) the expression of M1 macrophage markers iNOS and M2 macrophage markers Arg-1 were detected by RT-qPCR (N=5 in each group). The data are expressed as mean ± SD; one-way ANOVA and Tukey's post hoc test was used for comparison among multiple groups; and repeated measurement analysis of variance was used for data comparison between two groups at different time points; *, P<0.05. FOXP1, Forkhead Box P1; HE staining, hematoxylin-eosin staining; ELISA, enzyme-linked immunosorbent assay; IL-1β, interleukin-1β; IL-6, interleukin-6; TNF-α, tumor necrosis factor-α; IL-10, interleukin-10; BALF, bronchoalveolar lavage fluid; FSC, forward scatter; SSC, side scatter; PI, propidium iodide; iNOS, inducible nitric oxide synthase; Arg-1, Arginase-1; RT-qPCR, reverse transcription quantitative polymerase chain reaction; SD, standard deviation; ANOVA, analysis of variance; ns, no significance.

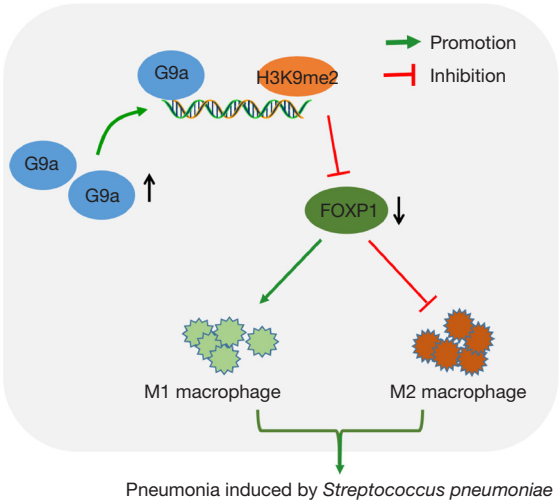

Figure 8 G9a can promote M1 polarization and inhibit M2 polarization of macrophages by promoting H3K9me2 methylation in FOXP1 promoter region to inhibit its transcription, thus promoting inflammatory response in Streptococcus pneumoniae induced pneumonia. H3K9me2, histone 3 lysine 9 dimethylation; FOXP1, Forkhead Box P1.

in the BALF were decreased, while IL-10 was elevated. Epigenetic changes are linked to lymphocyte movement, as *G9a* depletion blocks T-cell migration (32), and inhibition of G9a-associated pathways produced systematic mitigation of inflammation and suppression of viral replication (33). These results suggest *G9a* knockdown repressed inflammation in Spn mice.

Macrophages are important for modulating the antibacterial function of neutrophils and eradicating infection (34). The polarization from M1 macrophages to M2 macrophages can reduce the inflammatory reaction, promote tissue repair and regeneration, control excessive inflammatory reaction, and maintain the balance between pro-inflammatory and anti-inflammatory reactions (26). To further explore whether *G9a* could affect the polarization of pulmonary macrophages *in vivo*, we examined CD86 and CD206 expression in lung tissue. Flow cytometry and RT-qPCR elicited CD86 was notably decreased and CD206 was increased, while *iNOS* was lowered and *Arg-1* was significantly elevated after *G9a* knockdown. CD206 is predominantly expressed on the surface of activated macrophages where it is of paramount significance in innate and adaptive immunity in pneumonia (35). M2 macrophages have anti-inflammatory functions to eliminate excess inflammation (35), and *G9a* knockdown promoted the polarization of M1 macrophages to M2 macrophages *in vivo*. Moreover, LPS-induced RAW264.7 macrophages were delivered with sh-G9a, and *G9a* knockdown *in vitro* consistently and significantly inhibited polarization of M1 macrophages in LPS-induced RAW264.7 macrophages. There is no report on the role of G9a in macrophage polarization in pneumonia, which indicated the novelty of our study.

Treatment of macrophages with LPS in the presence or absence of interferon-γ (IFN-γ) to induce a 'M1-like' activated phenotype or with IL-4 to induce an 'M2-like' activated phenotype have been extensively used as in vitro paradigms for investigation of signal-dependent gene expression and metabolic reprogramming (36). The LPS response in macrophages is initially driven by latent transcription factors that include nuclear factor kappa-B (NF-κB), activating protein-1 (AP-1) and IRFs that subsequently result in secondary transcriptional responses to type I interferons and other cytokines. Also, LPS-induced changes in histone lysine methylation result in gene-specific transcription for regulation of inflammation (37). In LPS-induced macrophages, PHF8 knockdown leads to reduction of pro-inflammatory factors and increases in H3K9me2 written by G9a (37), and G9a inhibits FOXP1 by promoting H3K9me2 methylation in lung cancer (15). As FOXP1 is related to pathogen sensing, neutrophils and macrophages recruitment and inflammatory processes (27), we speculated G9a affected pneumonia through epigenetic regulation of FOXP1 transcription in Spn mice. The ChIP experiment showed the enrichment of H3K9me2 in the FOXP1 promoter region in RAW264.7 macrophages was decreased after *G9a* knockdown, and after addition of Bix01294 [a specific inhibitor of G9a (H3K9me2)] to cells, the enrichment of H3K9me2 in the FOXP1 promoter region was evidently inhibited. An epigenetic modifier, G9a is known to increase H3K9me2 (30,38), and RT-qPCR showed that FOXP1 transcription was increased clearly after *G9a* depletion. FOXP1 expression was also decreased in the Spn group but increased after *G9a* depletion. Overall, G9a inhibits FOXP1 transcription by promoting H3K9me2 methylation in the FOXP1 promoter.

FOXP1 is involved in lung infection and P. aeruginosa-induced pneumonia (27). To further study whether G9a affects macrophage polarization by inhibiting FOXP1 transcription, we treated RAW264.7 macrophages in the sh-

G9a group with sh-FOXP1. Flow cytometry revealed CD86 was increased and CD206 was decreased, and RT-qPCR elicited that *iNOS* was increased and *Arg-1* was decreased after simultaneously silencing G9a and FOXP1. Foxp3+ regulatory T cells promote recovery from severe pneumonia in mice (39), and downregulation of FOXP1 might trigger the secretion of IL-1β and IL-6 (40) and is required for monocyte differentiation and macrophage function (41,42). Taken together, FOXP1 silencing *in vitro* can avert the inhibitory effect of *G9a* knockdown on M1 macrophages. Consistently, the *in vivo* experiments elicited that after simultaneously silencing G9a and FOXP1, the weight of Spn mice was reduced, the pathological injury of lung tissue and inflammation were aggravated, CD86 was increased, CD206 was decreased, *iNOS* was increased, and *Arg-1* was decreased. Collectively, FOXP1 silencing *in vivo* can avert the protective effect of G9a inhibition on Spn mice.

In outbreak of COVID-19, among patients initially reported in Wuhan, the occurrence of macrophage activation syndrome, cytokine storm, and ARDS were heralded by very high levels of serum pro-inflammatory cytokines. Therefore, how to block the cytokine storm and when to initiate anti-inflammation therapy is critical for reducing death rate of COVID-19. The clinically severe phase of COVID-19 is accompanied by high levels of cytokine signaling (43). Thus, the inhibitors of signaling pathways and cytokines were investigated (44,45). Although the pathogen involved in this study is different from COVID-19, but both of them can eventually lead to sepsis and cytokine storm sharing similar pathway. Thus, G9a may play a critical role in the inflammation response in pneumonia and even become potential therapeutic target for COVID-19.

In summary, G9a promotes polarization of M1 to M2 macrophages by elevating H3K9me2 methylation in the FOXP1 promoter region to inhibit its transcription, promoting an inflammatory response in Spn mice. Macrophage polarization is monitored by several cellular and molecular mechanisms, including microRNAs (46,47). However, whether G9a-mediated FOXP1 transcription is regulated by microRNAs and whether G9a-targeted treatment can be applied in clinical methods for Spn management requires further investigation and validation.

Acknowledgments

Funding: This work was supported by Tianjin Health Science and Technology Project (No. 2020XKC07).

Footnote

Reporting Checklist: The authors have completed the ARRIVE reporting checklist. Available at https://atm.amegroups.com/article/view/10.21037/atm-22-1884/rc

Data Sharing Statement: Available at https://atm.amegroups.com/article/view/10.21037/atm-22-1884/dss

Conflicts of Interest: The authors have completed the ICMJE uniform disclosure form (available at https://atm.amegroups.com/article/view/10.21037/atm-22-1884/coif). All authors report that this work was supported by Tianjin Health Science and Technology Project (No. 2020XKC07). The authors have no other conflicts of interest to declare.

Ethical Statement: The authors are accountable for all aspects of the work in ensuring that questions related to the accuracy or integrity of any part of the work are appropriately investigated and resolved. Animal experiments were approved by the Animal Ethics Committee of Tianjin Chest Hospital (No. TJCH-2021-010), in compliance with Chinese national guidelines for the care and use of animals.

References

1. Guo X, Sun Q, Xi H, et al. Expression, purification, and characterization of pneumococcal PsaA-PspA fusion protein. Protein Expr Purif 2021;178:105782.
2. Jahn K, Handtke S, Palankar R, et al. Pneumolysin induces platelet destruction, not platelet activation, which can be prevented by immunoglobulin preparations in vitro. Blood Adv 2020;4:6315-26.
3. Dorosti H, Nezafat N, Heidari R, et al. Production and Immunological Evaluation of Epitope-based Preventative Pneumococcal Candidate Vaccine Comprising Immunodominant Epitopes from PspA, CbpA, PhtD and PiuA Antigens. Curr Pharm Biotechnol 2021;22:1900-9.

4. Myhre HO. Surgical treatment of aorto-iliac atherosclerosis. Acta Chir Scand 1977;143:15-20.
5. Chang PY, Tsao SM, Chang JH, et al. Plasma levels of soluble intercellular adhesion molecule-1 as a biomarker for disease severity of patients with community-acquired pneumonia. Clin Chim Acta 2016;463:174-80.
6. Murray PJ, Wynn TA. Protective and pathogenic functions of macrophage subsets. Nat Rev Immunol 2011;11:723-37.
7. Hume DA, Freeman TC. Transcriptomic analysis of mononuclear phagocyte differentiation and activation. Immunol Rev 2014;262:74-84.
8. Huang S, Zhu B, Cheon IS, et al. PPAR-γ in Macrophages Limits Pulmonary Inflammation and Promotes Host Recovery following Respiratory Viral Infection. J Virol 2019;93:e00030-19.
9. Brown TA, Lee JW, Holian A, et al. Alterations in DNA methylation corresponding with lung inflammation and as a biomarker for disease development after MWCNT exposure. Nanotoxicology 2016;10:453-61.
10. Shinjo K, Kondo Y. Clinical implications of epigenetic alterations in human thoracic malignancies: epigenetic alterations in lung cancer. Methods Mol Biol 2012;863:221-39.
11. Unoki M. Current and potential anticancer drugs targeting members of the UHRF1 complex including epigenetic modifiers. Recent Pat Anticancer Drug Discov 2011;6:116-30.
12. Cao H, Li L, Yang D, et al. Recent progress in histone methyltransferase (G9a) inhibitors as anticancer agents. Eur J Med Chem 2019;179:537-46.
13. Scheer S, Zaph C. The Lysine Methyltransferase G9a in Immune Cell Differentiation and Function. Front Immunol 2017;8:429.
14. Jan S, Dar MI, Wani R, et al. Targeting EHMT2/ G9a for cancer therapy: Progress and perspective. Eur J Pharmacol 2021;893:173827.
15. Pangeni RP, Yang L, Zhang K, et al. G9a regulates tumorigenicity and stemness through genome-wide DNA methylation reprogramming in non-small cell lung cancer. Clin Epigenetics 2020;12:88.
16. Ligresti G, Caporarello N, Meridew JA, et al. CBX5/ G9a/H3K9me-mediated gene repression is essential to fibroblast activation during lung fibrosis. JCI Insight 2019;5:127111.
17. Wang X, Chen S, He J, et al. Histone methyltransferases G9a mediated lipid-induced M1 macrophage polarization through negatively regulating CD36. Metabolism 2021;114:154404.
18. Zhang Y, Song D, Peng Z, et al. Anisodamine enhances macrophage M2 polarization through suppressing G9a-mediated IRF4 silencing to alleviate LPS-induced acute lung injury. J Pharmacol Exp Ther 2022. [Epub ahead of print].
19. Wang G, Fu Y, Ma K, et al. NOD2 regulates microglial inflammation through the TAK1-NF-κB pathway and autophagy activation in murine pneumococcal meningitis. Brain Res Bull 2020;158:20-30.
20. Lauw FN, Branger J, Florquin S, et al. IL-18 improves the early antimicrobial host response to pneumococcal pneumonia. J Immunol 2002;168:372-8.
21. Zhang Z, Li X, Sun W, et al. Loss of exosomal miR-320a from cancer-associated fibroblasts contributes to HCC proliferation and metastasis. Cancer Lett 2017;397:33-42.
22. Mümmler C, Burgy O, Hermann S, et al. Cell-specific expression of runt-related transcription factor 2 contributes to pulmonary fibrosis. FASEB J 2018;32:703-16.
23. Kim JH, Kim K, Youn BU, et al. Kruppel-like factor 4 attenuates osteoblast formation, function, and cross talk with osteoclasts. J Cell Biol 2014;204:1063-74.
24. Sun T, Zhang K, Pangeni RP, et al. G9a Promotes Invasion and Metastasis of Non-Small Cell Lung Cancer through Enhancing Focal Adhesion Kinase Activation via NF-κB Signaling Pathway. Mol Cancer Res 2021;19:429-40.
25. Dukhinova M, Kokinos E, Kuchur P, et al. Macrophage-derived cytokines in pneumonia: Linking cellular immunology and genetics. Cytokine Growth Factor Rev 2021;59:46-61.
26. Herold S, Mayer K, Lohmeyer J. Acute lung injury: how macrophages orchestrate resolution of inflammation and tissue repair. Front Immunol 2011;2:65.
27. De Simone M, Spagnuolo L, Lorè NI, et al. Mapping genetic determinants of host susceptibility to Pseudomonas aeruginosa lung infection in mice. BMC Genomics 2016;17:351.
28. Yang H, Yang Z, Mao Z, et al. Genome-Wide DNA Methylation Analysis of Soybean Curled-Cotyledons Mutant and Functional Evaluation of a Homeodomain-Leucine Zipper (HD-Zip) I Gene GmHDZ20. Front Plant Sci 2021;11:593999.
29. Kapazoglou A, Tani E, Avramidou EV, et al. Epigenetic Changes and Transcriptional Reprogramming Upon Woody Plant Grafting for Crop Sustainability in a Changing Environment. Front Plant Sci 2021;11:613004.
30. Pande P, Zhong XB, Ku WW. Histone Methyltransferase G9a Regulates Expression of Nuclear Receptors and Cytochrome P450 Enzymes in HepaRG Cells at Basal

Level and in Fatty Acid Induced Steatosis. Drug Metab Dispos 2020;48:1321-9.
31. Liu W, Meridew JA, Aravamudhan A, et al. Targeted regulation of fibroblast state by CRISPR-mediated CEBPA expression. Respir Res 2019;20:281.
32. Zhang X, Cook PC, Zindy E, et al. Integrin α4β1 controls G9a activity that regulates epigenetic changes and nuclear properties required for lymphocyte migration. Nucleic Acids Res 2016;44:3031-44.
33. Wang L, Muneer A, Xie L, et al. Novel gene-specific translation mechanism of dysregulated, chronic inflammation reveals promising, multifaceted COVID-19 therapeutics. bioRxiv 2020. Nov 16; 2020.11.14.382416.
34. Lee HH, Aslanyan L, Vidyasagar A, et al. Depletion of Alveolar Macrophages Increases Pulmonary Neutrophil Infiltration, Tissue Damage, and Sepsis in a Murine Model of Acinetobacter baumannii Pneumonia. Infect Immun 2020;88:e00128-20.
35. Tsuchiya K, Suzuki Y, Yoshimura K, et al. Macrophage Mannose Receptor CD206 Predicts Prognosis in Community-acquired Pneumonia. Sci Rep 2019;9:18750.
36. O'Neill LA, Pearce EJ. Immunometabolism governs dendritic cell and macrophage function. J Exp Med 2016;213:15-23.
37. Erdoğan Ö, Xie L, Wang L, et al. Proteomic dissection of LPS-inducible, PHF8-dependent secretome reveals novel roles of PHF8 in TLR4-induced acute inflammation and T cell proliferation. Sci Rep 2016;6:24833.
38. Lu H, Lei X, Zhang Q. Liver-specific knockout of histone methyltransferase G9a impairs liver maturation and dysregulates inflammatory, cytoprotective, and drug-processing genes. Xenobiotica 2019;49:740-52.
39. Walter JM, Helmin KA, Abdala-Valencia H, et al. Multidimensional assessment of alveolar T cells in critically ill patients. JCI Insight 2018;3:e123287.
40. Song Y, Li Q, Liao S, et al. Epstein-Barr virus-encoded miR-BART11 promotes tumor-associated macrophage-induced epithelial-mesenchymal transition via targeting FOXP1 in gastric cancer. Virology 2020;548:6-16.
41. Shi C, Sakuma M, Mooroka T, et al. Down-regulation of the forkhead transcription factor Foxp1 is required for monocyte differentiation and macrophage function. Blood 2008;112:4699-711.
42. Mulvaney EP, O'Sullivan ÁG, Eivers SB, et al. Differential expression of the TPα and TPβ isoforms of the human T Prostanoid receptor during chronic inflammation of the prostate: Role for FOXP1 in the transcriptional regulation of TPβ during monocyte-macrophage differentiation. Exp Mol Pathol 2019;110:104277.
43. Keystone EC, Taylor PC, Drescher E, et al. Safety and efficacy of baricitinib at 24 weeks in patients with rheumatoid arthritis who have had an inadequate response to methotrexate. Ann Rheum Dis 2015;74:333-40.
44. Jamilloux Y, El Jammal T, Vuitton L, et al. JAK inhibitors for the treatment of autoimmune and inflammatory diseases. Autoimmun Rev 2019;18:102390.
45. Ding C, Jones G. Anti-interleukin-6 receptor antibody treatment in inflammatory autoimmune diseases. Rev Recent Clin Trials 2006;1:193-200.
46. Madhyastha R, Madhyastha H, Nurrahmah QI, et al. MicroRNA 21 Elicits a Pro-inflammatory Response in Macrophages, with Exosomes Functioning as Delivery Vehicles. Inflammation 2021;44:1274-87.
47. Chambers M, Rees A, Cronin JG, et al. Macrophage Plasticity in Reproduction and Environmental Influences on Their Function. Front Immunol 2021;11:607328.

Cite this article as: Li Y, Li G, Zhang L, Li Y, Zhao Z. G9a promotes inflammation in *Streptococcus pneumoniae* induced pneumonia mice by stimulating M1 macrophage polarization and H3K9me2 methylation in FOXP1 promoter region. Ann Transl Med 2022;10(10):583. doi: 10.21037/atm-22-1884

